X-Ray-Based Attenuation Correction for Positron Emission Tomography/Computed Tomography Scanners

Paul E. Kinahan, Bruce H. Hasegawa, and Thomas Beyer

A synergy of positron emission tomography (PET)/computed tomography (CT) scanners is the use of the CT data for x-ray-based attenuation correction of the PET emission data. Current methods of measuring transmission use positron sources, gamma-ray sources, or x-ray sources. Each of the types of transmission scans involves different trade-offs of noise versus bias, with positron transmission scans having the highest noise but lowest bias, whereas x-ray scans have negligible noise but the potential for increased quantitative errors. The use of x-ray-based attenuation correction, however, has other advantages, including a lack of bias introduced from post-injection transmission scanning, which is an important practical consideration for clinical scanners, as well as reduced scan times. The sensitivity of x-ray-based attenuation correction to artifacts and quantitative errors depends on the method of translating the CT image from the effective x-ray energy of ~70 keV to attenuation coefficients at the PET energy of 511 keV. These translation methods are usually based on segmentation and/or scaling techniques. Errors in the PET emission image arise from positional mismatches caused by patient motion or respiration differences between the PET and CT scans; incorrect calculation of attenuation coefficients for CT contrast agents or metallic implants; or keeping the patient's arms in the field of view, which leads to truncation and/or beam-hardening (or x-ray scatter) artifacts. Proper interpretation of PET emission images corrected for attenuation by using the CT image relies on an understanding of the potential artifacts. In cases where an artifact or bias is suspected, careful inspection of all three available images (CT and PET emission with and without attenuation correction) is recommended.

THE PRIMARY PURPOSE of combining x-ray computed tomography (CT) and positron emission tomography (PET) scanners is for the precise anatomical localization of regions identified on the PET tracer uptake images.[1,2] As discussed by Townsend et al (page 193) in this issue, a synergism with PET/CT scanners is the use of the CT scanner for x-ray-based attenuation correction of the PET emission data.[3] All manufacturers of PET/CT scanners incorporate x-ray CT based attenuation correction algorithms in their systems, and for some PET/CT scanners it is the only option offered. We review attenuation correction for PET/CT scanners, starting with a brief explanation of the nature of attenuation in x-ray and nuclear medical imaging. Next we contrast the possible methods of measuring the needed transmission data. We then discuss possible approaches to CT-based transmission measurements and conclude with a discussion of the advantages and challenges of using CT-based attenuation correction with PET/CT scanners.

The Need for Attenuation Correction

Several physical effects can perturb tracer uptake images that were obtained with PET.[4] The most significant of these effects are photon attenuation, scattered and random coincidences, detector efficiency variations, and scanner deadtime. Of these, by far the most important is photon attenuation, which can affect both the visual quality and the quantitative accuracy of PET data. Figure 1 is an example of an [^{18}F]-fluorodeoxyglucose (FDG) PET scan in which lesion detection is significantly degraded in the image reconstructed without compensation for photon attenuation (Fig 1c) in comparison with the image reconstructed with attenuation correction (Fig 1b).

It is difficult to mathematically predict the specific appearance of PET images reconstructed without attenuation compensation. It is possible, however, to predict some common artifacts such as enhanced activity in pulmonary regions (that is, "hot lungs") and negative tracer concentrations in mediastinal regions[5] in uncorrected images. In regions of non-uniform density, such as the thorax, the lack of attenuation correction can mask the appearance of solid lesions with moderately elevated tracer uptake[6] in the resultant images (for example Fig 1c).

There has been considerable debate about the desirability of attenuation correction in whole-body PET oncology imaging.[7] Some *perceived* advantages of reconstructing images without attenuation correction are avoiding noise amplification, reducing patient scanning time, and improved contrast/noise ratios for lesions. These perceptions are incorrect, as discussed by Bai et al.[5] There are, however, valid reasons for reconstructing PET images without attenuation correction: checking for the presence of artifacts introduced by patient motion occurring between the emission and transmission scans and/or mechanical problems with the transmission scan and the additional anatomical information available in the non-corrected image. In many centers, the PET images

From the University of Washington, Seattle, WA; University of California at San Francisco, San Francisco, CA; University Hospital of Essen, Germany.

Address reprint requests to: Corresponding author: Paul Kinahan, PhD, University of Washington Medical Center, Box 356004, RM NW040, 1959 NE Pacific St., Seattle, WA 98195-6004.

This work was supported by NIH grant CA74135 from the National Cancer Institute.

0001-2998/03/3303-0001$30.00/0

doi:10.1053/snuc.2003.127307

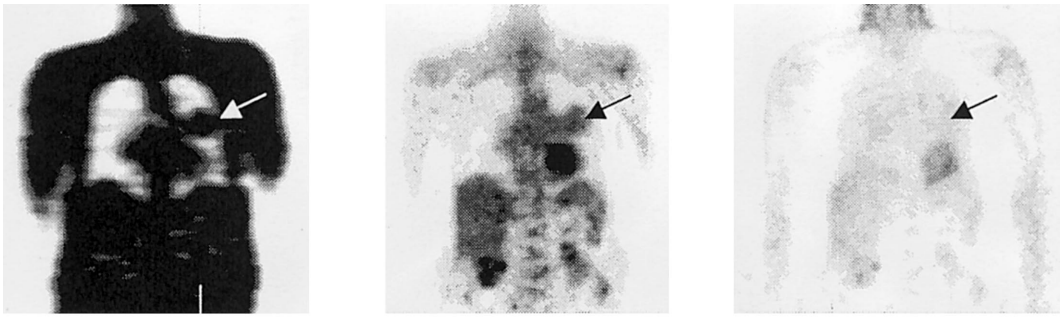

(a) Transmission (attenuation) image

(b) FDG uptake image with correction for attenuation

(c) FDG uptake image without correction for attenuation

Fig 1. Example of FDG uptake with and without attenuation correction. (a) A harmatoma (arrow) is visible in the transmission image, also called an attenuation image, and (b) in the FDG image with attenuation correction, but is not visible (c) in the FDG image without attenuation correction.

with and without attenuation correction are, therefore, considered to provide complementary information.

ATTENUATION

Transmission of photons through any material can be characterized by the linear attenuation coefficient μ, which depends on the photon energy E and the atomic number Z of the material. The linear attenuation coefficient can be defined as the probability per unit pathlength that the photon will interact with the absorber (for example, patient tissue). The general concept of photon attenuation incorporates two types of interaction: absorption and scatter. For an ideal narrow beam of mono-energetic photons, the resulting fractional reduction of the beam intensity $-dI/I$ through an absorber having a linear attenuation coefficient μ is proportional to the absorber thickness dt, that is, $-dI/I$, which can be integrated to obtain

$$I(t) = I_0 \exp\left(-\int_0^t \mu dt'\right) \quad (1)$$

where I_0 is the incident beam intensity. For homogeneous materials this reduces to the well-known Bouger-Lambert-Beer law: $I(t) = I_0 \exp(-\mu t)$.

Linear attenuation coefficients are expressed in units of inverse centimeters (cm^{-1}) and are proportional to the density ρ of the absorber. It is, therefore, common to express the attenuation property of a material in terms of its *mass attenuation coefficient* μ/ρ in units of cm^2/g.[8] The total attenuation coefficient (that is, either total linear attenuation coefficient or total mass attenuation coefficient) for an interaction is given by the sum of the possible photon interaction mechanisms, which for diagnostic imaging are primarily caused by photoelectric absorption and Compton scattering.

The mass attenuation coefficient for photoelectric absorption varies approximately as

$$\frac{\mu}{\rho} \alpha \frac{Z^{4.5}}{E^3}, \quad (2)$$

for atomic numbers from $Z = 1$ to 92 (uranium) and for photon energies from $E = 10$ to 500 keV, thus demonstrating a strong dependence on both photon energy and material.[9] The attenuation coefficient for photoelectric absorption also has discrete discontinuities at photon energies corresponding to the ejection of specific inner-shell electrons from the atom following photon absorption. In comparison, the linear attenuation coefficient for Compton scattering is directly proportional to Z and has a slight inverse dependence (albeit nonlinear) on photon energy between 10 and 1000 keV.[10] The total, photoelectric, and Compton linear attenuation coefficients for muscle and bone, in the range of 10 to 1000 keV, are shown in Fig 2. The total attenuation is dominated by the photoelectric effect below photon energies of 30 keV and 50 keV for soft-tissue and bone and is dominated by Compton scattering for photon energies between 200 to 1000 keV. These characteristics are important in com-

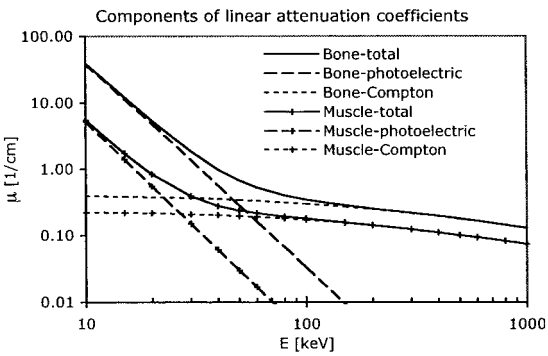

Fig 2. Linear attenuation coefficients for bone and muscle in the range of 10 to 1000 keV. The photoelectric absorption and Compton scattering components are also shown. The total attenuation coefficient accounts for all photon interactions, not just photoelectric absorption and Compton scattering.[9]

paring x-ray and PET transmission scans of bone and other high-Z materials.

The mass attenuation coefficients for several materials are shown in Fig 3 for photon energies from 10 to 1000 keV. As noted above, the linear attenuation coefficient (μ) for Compton scattering is proportional to the atomic number, making the mass attenuation coefficient (μ/ρ) for Compton scattering essentially independent of material type. Therefore, the mass attenuation coefficient for different materials converges for photon energies between 200 to 1000 keV where Compton scattering dominates. radiograph imaging occurs in the energy range from 30 to 130 keV and is determined by both photoelectric absorption and Compton scatter, whereas PET imaging occurs at 511 keV where photon attenuation by biological materials is determined solely by Compton scattering.

For other compounds, including body-equivalent plastics,[12] or body regions represented by combinations of air and soft tissue (lung) or combinations of soft tissue and bone, the mass attenuation coefficient can be calculated according to the mixture rule

$$\frac{\mu}{\rho} = \sum_i \frac{w_i \mu_i}{\rho_i} \tag{3}$$

where w_i is the proportion by weight of the i-th constituent. The mixture rule is accurate to within a few percent for photon energies above 10 keV.

Photon Energy Spectra

The relative contribution of Compton scattering and photoelectric absorption for x-ray imaging of a given material is determined by the continuous *bremsstrahlung* ("braking radiation") spectrum produced by bombarding a target, typically tungsten, with high energy electrons. The x-ray spectrum also contains characteristic x-rays having discrete energies corresponding to the transition of orbital electrons in the target material. In comparison, PET imaging is performed by detecting mono-energetic annihilation photons produced by electron-positron annihilations. Each photon has an energy equal to the electron and positron mass (511 keV). The third type of

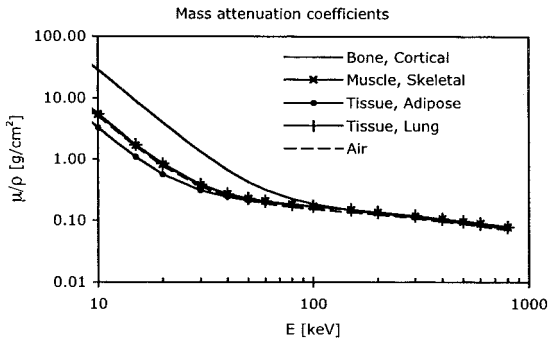

Fig 3. Total mass attenuation coefficients for several biological materials.[11]

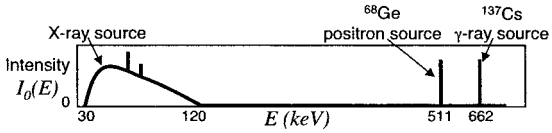

Fig 4. Illustration of the spectral distributions for x-ray and PET imaging. Not to scale.

photons, γ-rays, are produced by atomic nuclei and have discrete energies determined by nuclear transitions. A schematic illustration of the energy spectra from an x-ray source, a positron source (^{68}Ge/^{68}Ga), and a typical γ-ray source (^{137}Cs) is shown in Fig 4.

X-ray CT uses detectors that are operated in the charge-integration mode without energy discrimination. This contrasts with radionuclide imaging (including PET), which relies on detectors with energy-discrimination to assist in rejecting scatter. Therefore, the intensity I of a polyenergetic photon beam transmitted through an absorber of finite thickness (for example, tissues in the body) can be represented by

$$I = \int_0^{E_{\max}} I(E)dE = \int_0^{E_{\max}} I_0(E)\exp\left(-\int_{-\infty}^{\infty} \mu(t,E)dt'\right)dE \tag{4}$$

where the limits of integration with respect to t are $\pm\infty$ because the object (that is, the patient cross-section) is finite in size. For x-ray imaging, $I_0(E)$ describes the spectrum of the incident x-ray beam, I represents the intensity of the transmitted beam, and $E_{\max}$ is the accelerating voltage of the x-ray tube (for example, 120 kVp in Fig 4). Because low-energy photons are preferentially absorbed when passing through matter (Eq. 2), the energy spectrum is shifted toward higher photon energies. This produces the well known *beam-hardening* effect, where thick or dense body regions transmit photons with a "hardened" spectrum (that is, having a larger proportion of higher energy photons) in comparison with low-attenuating or thin regions. Beam-hardening effects can introduce contrast variations that depend on the choice of x-ray path through a region of the body, rather than by the local tissue characteristics of the region itself. In other words, CT image values would vary locally as a function of patient size, as well as the intrinsic attenuation coefficients, clearly an undesirable behavior.

TOMOGRAPHIC IMAGING

Mono-Energetic Transmission Imaging

The process of generating a patient-specific attenuation map begins with the acquisition of transmission data by using an external source of radiation. The imaging geometry is illustrated in Fig 5 in which radiation from an external source with an incident intensity of I_o is transmitted through an object represented by a two-dimensional distribution of linear attenuation coeffi-

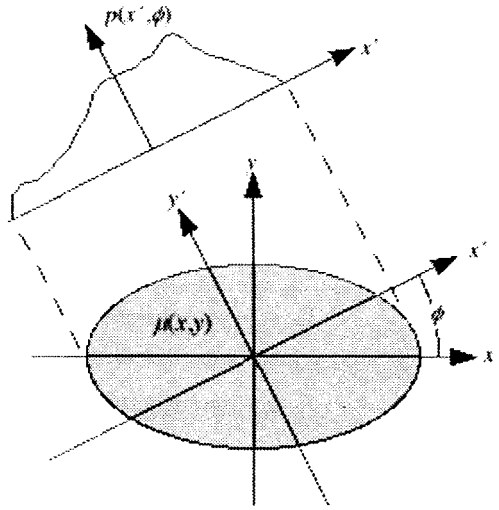

Fig 5. Geometry used for projections of the attenuation object for Eq. 5.

cients $\mu = \mu(x,y)$. As the radiation passes through the object, it is attenuated so that the transmitted intensity distribution $I(x',\phi)$ is recorded by the detector, where x', is the distance along the detector array. This process is repeated at multiple angles ϕ, measured with respect to the x-axis of the object.

If we use a mono-energetic ($E = E_0$) photon source to acquire the transmission data, we can use Eq. (1) to relate the acquired detector signals I to the attenuation coefficient. By taking the logarithmic ratio we obtain

$$p(x',\phi) = \ln\left(\frac{I_0}{I(x',\phi)}\right) = \int_{-\infty}^{\infty} \mu(x,y,E_0)dy' \qquad (5)$$

where $p(x',\phi)$ is the *projection*, or sinogram, of the acquired data, and where the integral equation represented by Eq. 5 is known as the x-ray or radon transform. Tomographic image reconstruction performs the inverse operation of Eq. 5 to obtain an estimate of $\mu = \mu(x,y)$ from the set of all $p(x',\phi)$. Tomographic reconstruction is a well-understood problem, for which the best known solution is the filtered-backprojection (FBP) algorithm.[13] Other reconstruction methods, usually iterative, include mathematical models of the underlying physics of the image acquisition process, including photon attenuation, Poisson statistics, scatter radiation, and the geometric response of the detector. These reconstruction methods have the potential to improve the signal to noise ratios (SNRs) of the reconstructed image.[14,15]

Polyenergetic Transmission Imaging

Although in CT the data acquisition geometry is similar to that shown in Fig 5, x-ray imaging is complicated by beam-hardening effects that arise from differential absorption of lower-energy photons as the polyenergetic x-ray beam passes through the object. As a result, beam hardening leads to transmission images in which the reconstructed attenuation value of a tissue depends on the location within the patient, as the photon energy spectra varies within the patient. Fortunately, beam hardening effects are corrected to a high degree of accuracy[16] in all modern CT scanners. Because this correction process does not provide an absolute calibration of the reconstructed attenuation coefficients, image values in the reconstructed CT image are scaled as Hounsfield units (HU) H

$$H(x,y) = 1000\left(\frac{\mu(x,y)}{\mu_{\text{water}}} - 1\right) \qquad (6)$$

which is the standard means of representing CT images from clinical scanners. In this scale, air has the value $H = -1000$, water has the value $H = 0$, and tissues denser than water have values $H > 0$. Compact bone, for example, typically has values in the range from 1000 to 2000, whereas adipose tissue has values near -100.

PET Emission Imaging

The physical process of photon attenuation obviously affects annihilation photons that are produced and detected in PET emission imaging. In PET imaging (Fig 6), the photon pairs produced by positron-electron annihilation travel in opposite directions (to conserve momentum) and are detected within a few nanoseconds of each other. In this case the positron source is known to lie somewhere on the *line of response* (LOR) between the detection points (A and B in Fig 6). This time-coincidence determination of the LOR gives PET its remarkable sensitivity because collimators are not needed to determine the orientation (x',ϕ) of the LOR. An added advantage of the collinear photons is that the total attenuation across the LOR is constant, regardless

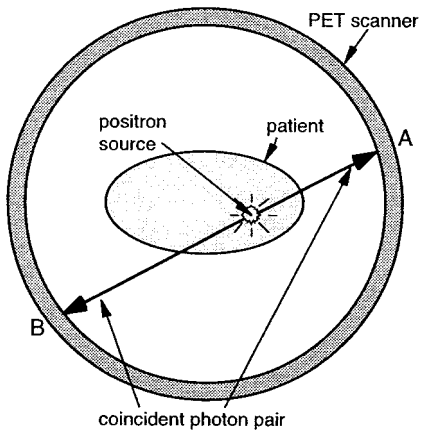

Fig 6. Process of PET emission imaging for a two-dimensional cross-section of the patient. When both 511 keV annihilation photons are detected in coincidence, then the positron source is known to lie on the LOR between the detection points A and B.

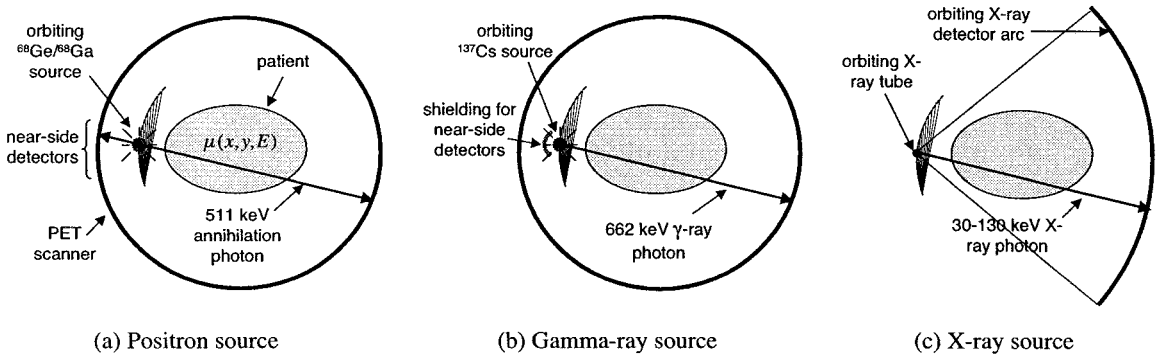

Fig 7. Illustration of the three modes of measuring attenuation factors through a patient cross section. Note that the attenuation coefficient is a function of position and energy.

of the location of the positron source along the LOR. This is easy to show mathematically by adding the attenuation of photons along line segments A and B, each according to Eq. 1.

Using the geometry depicted in Fig 5, the collected *emission* projection data can be represented by

$$p(x',\phi)=\left[\exp\left(-\int_{-\infty}^{\infty}\mu(x,y)dy'\right)\right]\int_{-\infty}^{\infty}f(x,y)dy' \quad (7)$$

where the exponential term (in square brackets) represents the attenuation along the LOR at detector position x' and projection angle ϕ, and where $f(x,y)$ represents the distribution of FDG or other positron tracer in the patient. The goal of PET imaging is to estimate the distribution of FDG uptake. More precisely, tomographic reconstruction is used to calculate $f(x,y)$ from the set of acquired projection data $p(x',\phi)$ represented by Eq. 7. The form of Eq. 7 can be simplified by expressing the inverse of the exponential term as an attenuation correction factor

$$a(x',\phi)=\exp\left(\int_{-\infty}^{\infty}\mu(x,y)dy'\right). \quad (8)$$

which represents inverse of the dual-photon attenuation along the LOR for detector position x' and projection angle ϕ. A multiplicative correction for photon attenuation is then given by

$$p_{AC}(x',\phi)=a(x',\phi)p(x',\phi)=\int_{-\infty}^{\infty}f(x,y)dy' \quad (9)$$

where $p_{AC}(x',\phi)$ are the emission data (sinograms) corrected for attenuation. Similar to Eq. 5 the corrected projection values $p_{AC}(x',\phi)$ can be used in a tomographic image reconstruction algorithm, such as FBP, to estimate the two-dimensional distribution of radionuclide concentration represented by the function $f(x,y)$. Alternatively, the acquired projection data $p(x,\phi)$ can be reconstructed directly with an iterative method, where the attenuation correction factors are used to provide proper statistical weighting to the data. An example of this approach is attenuation-weighted OSEM (AWOSEM),[17] which has been implemented on most commercial PET scanners.

DETERMINING ATTENUATION CORRECTION FACTORS

Calculated versus Measured Attenuation

As shown in Eqs. 8 and 9, attenuation correction factors $\alpha(x',\phi)$ must be derived from transmission data to correct the PET data for photon attenuation. If the object has a simple geometry and is homogeneous, then the attenuation correction factors for PET can be calculated assuming an a priori estimate of the object's geometry and knowledge of the materials (and their attenuation coefficients) in the object. This method avoids the need to acquire transmission data, but in practice is only marginally useful in brain imaging, where $\mu(x,y) = \mu_{water}$ can be assumed constant (that is, $\mu(x,y) = \mu_{water} = 0.096\ cm^{-1}$ at $E = 511$ keV). The skull boundaries can be estimated from a PET emission image reconstructed without attenuation correction. With the boundary information the attenuation correction factors can be calculated by using $\alpha(x',\phi) = \exp(-\mu l(x',\phi))$, where $l(x',\phi)$ is the chord length in cm of the intersection with the brain of the LOR indexed by (x',ϕ). This approach, however, introduces biases and will not work in heterogeneous anatomical regions such as the thorax, which contains a non-uniform distribution of attenuation coefficients. In this case, measured attenuation factors must be used.

The distribution of attenuation coefficients in the object can be measured by using transmission data that are measured by using positron sources, γ-ray sources, or x-ray sources (Fig 7). Comparing transmission scans with and without the patient in the field of view allows a direct estimate of the attenuation along each LOR. For attenuation correction, only the values of $\alpha(x',\phi)$ are

needed. There are cases, however, where it is useful to have the attenuation image $\mu(x,y)$, which can be obtained by reconstructing the data $\ln(\alpha(x',\phi)) = \int \mu(x,y)dy'$. The attenuation images might be segmented, for example, to suppress transmission noise. The processed attenuation image can then be used to generate attenuation correction factors according to Eq. 9.

Positron Sources

The transmission data needed to calculate the attenuation map can be recorded in coincidence-timing mode with a ^{68}Ge/^{68}Ga positron source.[18] The calculation (Eq. 6) requires that both a "blank" scan (that is, without a patient) and a transmission scan of the patient are acquired to calculate the attenuation coefficients at 511 keV. With coincidence scanning, however, the proximity of the positron source to the near-side detectors (Fig 7a) increases dead-time significantly. Some PET scanners only operate in high-sensitivity fully 3D mode,[19] where the absence of slice-defining septa further increases near-side detector dead-time. This can limit the positron source strength and the statistical quality of the transmission data and can propagate noise into the reconstructed image (Eq. 9). Scanners that have the option of operating in two-dimensional (2D) or fully 3D mode typically will collect transmission data in 2D mode. If fully 3D emission data are acquired then the full volume attenuation image $\mu(x,y,z)$ is first reconstructed and the necessary 3D attenuation correction factors calculated along the LORs, including those that were not measured, using the 3D extension of Eq. 8.[3,19] An advantage of using a positron source is that scattered or random events can be rejected by the "triple-point" method: using only those events for which the LOR of a detected event intersect the known location of the orbiting source.

It is possible to mitigate the statistical noise in transmission scan produced by a positron source by simple smoothing of the transmission data. This approach, however, can introduce significant noise correlations ("streaks") in the emission image if the type and degree of smoothing is not carefully matched to the noise levels in the transmission data. Alternatively the attenuation image $\mu(x,y)$ is reconstructed and then segmented, assuming homogenous regions.[20] Anatomical regions assumed to be of the same tissue type (for example, lung, soft-tissue, bone) then can be assigned with a constant attenuation coefficient representative of that material. Segmentation methods, however, have the potential to misclassify a voxel due to excessive noise, which can propagate errors into the emission image. A third approach is to use more sophisticated methods of transmission image reconstruction where the photon noise is carefully modeled (for example,[21]). These methods can result in improved SNR for the attenuation image, which is again used to generate attenuation correction factors with Eq. 8.

Gamma-Ray Sources

Although the methods described above use positron sources to acquire transmission data, it also is possible to use γ-ray sources (for example, ^{137}Cs) for this purpose. Single events can be recorded from a ^{137}Cs γ-ray source, thus, placed behind shielding for the near-side detectors (Fig 7b), allowing the use of a stronger photon transmission source, thus, yielding decreased noise in the transmission data.[22,23] In addition statistical reconstruction methods can also be implemented with single photon sources to further reduce statistical noise in transmission images.[24] This approach is particularly useful for PET scanners that can only operate in fully 3D acquisition mode where a positron source will yield in excessive noise levels in a transmission scan. Unfortunately the attenuation coefficients are not measured at 511 keV, but at the 662 keV photon energy of ^{137}Cs. To scale the measured attenuation coefficients down to 511 keV, both segmentation[25] and scaling approaches have been adopted.[26] An additional disadvantage of using the single photon source for transmission imaging is that these methods have an increased sensitivity to detecting scattered photons. The triple-point scatter rejection method is not available because the source location helps to determine the LOR although scatter correction methods can be applied to the transmission data.[26] In summary, ^{137}Cs single photon γ-ray sources offer reduced transmission noise, but at the potential cost of bias introduced by transforming the attenuation coefficients from 662 keV to 511 keV, and an increase in the fraction of scattered photons.

CT Sources

With PET/CT scanners a 511 keV attenuation map can be generated from the CT image to correct the PET emission data for photon attenuation.[3] There are four significant advantages of using CT to acquire transmission scans for attenuation correction of the PET emission data: First, the CT data will have much lower statistical noise, especially for whole-body PET imaging in comparison with transmission data acquired with radionuclide sources. Second, the CT scan can be acquired much more quickly than a standard PET transmission scan. Third is the ability to collect uncontaminated post-injection transmission scans, an important practical consideration. Radionuclide-based transmission scans suffer contamination from emission photons unless the transmission data are acquired before the PET agent is administered to the patient. In comparison, CT transmission scans can be acquired anytime after the PET tracer is injected because the x-ray photon flux is orders of magnitudes higher than the emission photon flux. This shortens the time spent by a patient on the scanner bed and provides more efficient use of scanner time by allowing overlapping of patient protocols. Fourth, using x-ray transmission scanning eliminates the need for PET

(a) ^{68}Ge/^{68}Ga positron source (b) ^{137}Cs gamma-ray source (c) 120 kVp x-ray source

Fig 8. Anecdotal illustrations of the three transmission methods used for measured attenuation correction for PET. In these images darker regions correspond to higher density (ie, bone).

transmission hardware and the periodic replacement of ^{68}Ge/^{68}Ga positron sources. A potential benefit not yet fully explored is the direct incorporation of anatomical information derived from the CT data into the PET image reconstruction process.[27]

When used to correct PET emission data for photon attenuation, attenuation coefficients measured with x-ray CT must be converted to the appropriate values at 511 keV. Once the attenuation map, $\mu(x,y,z)$, at the correct energy is obtained, the attenuation correction factor, $\alpha(x',\phi)$, for an individual sinogram element is calculated by numerically integrating $\mu(x,y,z)$ along the LOR corresponding to the emission sinogram element (Eq. 8). In comparison with positron and γ-ray sources, x-ray-based attenuation correction introduces negligible noise, but has increased potential for introducing bias in the reconstructed emission images. A differential comparison of the three methods is summarized by Fig 8 and Table 1.

The CT component of a PET/CT scanner would be used primarily for anatomical imaging and only secondarily for producing attenuation maps to correct the PET emission data. For these reasons the cost of the different transmission imaging techniques are not included in Table 1. The superior contrast and resolution of the CT image, important factors for anatomical imaging, are also not listed in Table 1 because the CT images are intentionally degraded to avoid introducing artifacts during attenuation correction.[3]

Figure 8 illustrates the differences in the characteristics of the image data obtained with the three techniques. Specifically, CT offers improved contrast, resolution, and noise characteristics in comparison with transmission images obtained with radionuclide sources. The improved contrast of CT is due to the larger fractional difference between attenuation coefficients of different tissues for the x-ray beam (30 to 140 keV) than for the radionuclide transmission source (511 or 662 keV) and by the significantly higher source strength used to acquire the CT image, which reduces photon statistical noise at the cost of higher radiation dose.

The use of x-ray-based attenuation correction has also been proposed and developed for dual SPECT/CT scanners.[28,29] One difference is that emission imaging with SPECT/CT commonly uses $^{99\ month}$Tc-labeled radiopharmaceuticals, which have a photon energy of 140 keV. Thus, scaling methods (discussed in the next section) to convert the CT image for attenuation correction of $^{99\ month}$Tc-SPECT images have been straightforward to implement for clinical imaging.[30,31]

X-RAY-BASED ATTENUATION CORRECTION METHODS

When 511 keV attenuation maps are generated from a CT patient image, the CT values are reconstructed in units of HU and cannot be directly used to correct the emission data for photon attenuation. There are three conversion methods: segmentation, scaling, and dual-energy CT scans.

Segmentation

Segmentation methods can be used to separate the CT image into regions corresponding to different tissue types (for example, soft tissue, lung, bone). The CT image values for each tissue type then are replaced with appropriate attenuation coefficients at a photon energy of 511 keV. A significant problem, however, is that some tissue regions will have continuously varying densities

Table 1. Comparison of the Three Transmission Methods Used for Measured Attenuation Correction for PET

Source	Positron	Single Photon γ-Ray	X-Ray
Photon energy (keV)	511	662 (for ^{137}Cs)	polyenergetic: ~30 to 140
Patient scan time (min)	~15-30	~5-10	~1
Transmission noise	highest	high	insignificant
Potential for bias/artifacts	low	some	highest

Note that scan times are approximate and estimated for an axial range of 75 cm.

that may not be accurately represented by a discrete set of segmented values. In pulmonary regions, for example, the density of lung tissue varies by as much as 30%.[32]

Scaling

In general, the image values produced by CT are approximately linearly related to the physical attenuation coefficient of the corresponding tissue type. For this reason, it is possible to estimate the attenuation map of the patient at 511 keV simply by multiplying the entire CT image by the ratio of attenuation coefficients of water (representing soft tissues) at the photon energies of CT and PET. A single "effective" energy is estimated to represent the CT spectrum, typically ~70 keV. LaCroix et al[29] performed simulation studies to investigate different techniques for scaling the attenuation coefficients from CT energies to 140 keV for SPECT. They found that linear scaling leads to proper attenuation coefficients for low-Z materials (for example air, water, and soft tissue). For bone, however, linear scaling is a poor approximation because photoelectric contributions dominate at the lower CT energies (Fig 2). In other words, different scaling factors for bone and soft tissue are needed to transform CT images acquired at an effective energy of approximately 70 keV to calculate an attenuation map calibrated at the emission energy of 511 keV.

One approach to compensate for the high-Z materials is to note that CT numbers in the range of $-1000 < H < 0$ primarily represent regions that contain mixtures of lung and soft tissue, whereas regions having CT numbers $H > 0$ are those that contain mixtures of soft-tissue and bone. Blankespoor et al[30] argued that a bilinear scaling could be used to convert CT images to 140 keV for attenuation correction of SPECT data. In this method, different scaling factors (for water and air and for water and bone) are used to calculate the attenuation values for CT numbers H, for which $-1000 < H < 0$, and for $H > 0$, respectively. The resulting attenuation values are illustrated in Fig 9 for linear attenuation coefficients at 511 keV for PET. This approach was recently proposed for PET by Burger and coworkers[33] and Bai et al.[34]

An alternative approach for converting CT images to attenuation maps is the "hybrid method," which combines segmentation and scaling.[3] The attenuation map at 511 keV is estimated by first using a threshold to separate out the bone component of the CT image, and then using separate scaling factors for the mass attenuation coefficients of the bone and non-bone components. This approach is motivated by Fig 3, where the ratio of mass attenuation coefficients from 70 to 511 keV for all materials except bone is the same. This is due to a larger photoelectric fraction caused by the large calcium fraction (~22.5% in cortical bone[12]) as described by Eq. 3, where $Z = 20$ for calcium. The behavior of the hybrid method in converting CT numbers to linear attenuation coefficients at 511 keV is contrasted with the bilinear scaling method in Fig 9, where the threshold for differentiating bone from non-bone regions was selected to be 300 HU, based on heuristic arguments.[3] Just as the bilinear method can be considered as combining an air/water mixture model for $-1000 < H < 0$ and a water/bone mixture model for $H > 0$, the hybrid method can also be considered as an air/water mixture model for $-1000 < H < 300$ and an air/bone mixture model for $H > 300$. This can be seen by extrapolating the $H > 300$ segment to $H = 0$. The resulting change in scale factors leads to a discontinuity at the threshold value as seen in Fig 9.

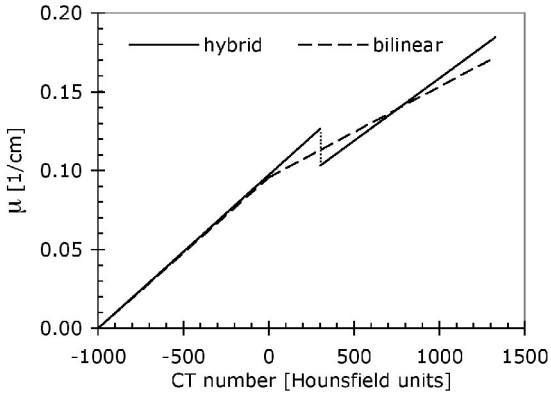

Fig 9. Conversion of CT numbers to linear attenuation coefficients at 511 keV. Note that there is a change in slope for the bilinear method at 0 HU and a discontinuity in the hybrid approach at 300 HU.

Although the hybrid method is not piece-wise continuous, unlike the bilinear method, there is no unique transformation from CT energies to 511 keV due to the possibility of independent variations in density and Z, which can cause two materials with similar CT values at some effective energy, say 70 keV, to have different attenuation coefficients at 511 keV. Conversely, it is possible for two distinct materials with the same value of attenuation coefficient at 511 keV to yield different CT numbers. Fortunately both the bilinear scaling method and the hybrid method methods have been shown to give reasonable results for biological materials in practice.[1,33,35] Recent studies have compared, in patients, transmission imaging with both positron and x-ray sources.[36,37] The effect on the reconstructed FDG emission images of the choice of transmission source was in general minor or insignificant, although this is not necessarily true when the patient contains contrast agents or metal objects.

Dual Energy X-Ray Imaging

An accurate solution to the problem of converting CT numbers to linear attenuation coefficients at 511 keV can be obtained by collecting two (or more) scans generated with x-ray beams with different energy spectra. This can be understood by regarding the attenuation coefficient as a weighted sum of photo-

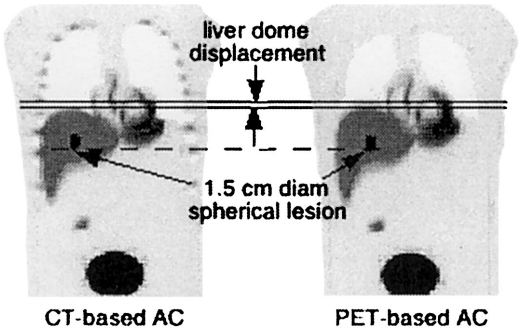

Fig 10. A noiseless simulation of the effect of respiration on CT-based attenuation correction as compared with a standard PET transmission scan. In the PET emission data a 1.5-cm diameter lesion (4:1 contrast) has been simulated. The appearance of the lesion is blurred axially due to respiration during the PET emission scan. The CT scan was acquired during maximum inspiration which has a spatial mismatch with the respiratory averaged PET emission and transmission scans. The result of using the CT-based attenuation correction is an apparent axial shift of the top of the liver dome. Data courtesy of Roberto Isoardi, PhD, and Claude Comtat, PhD.

electric absorption and Compton scattering probabilities, in essence a system with two components. If we were able to determine the individual photoelectric and Compton components, they could be scaled separately to any energy and then added to obtain the total attenuation coefficient. Such a quantitative CT imaging process was developed by Alvarez and Macovski.[38] This approach was used to form a monoenergetic attenuation map at 140 keV by Hasegawa and coworkers for a prototype SPECT/CT detector block.[29] A potential disadvantage is that the dual-energy CT method calculates the attenuation map by forming a generalized subtraction of the two separate CT scans, in which the noise of the component CT scans adds in quadrature. Therefore, although dual-energy techniques theoretically offer the highest degree of accuracy, they also can have degraded SNR characteristics in comparison with attenuation maps calculated from a single CT or radionuclide transmission scan if the patient radiation dose is kept constant.

Table 2. Measured Attenuation (HU) in Abdominal CT Images (Fig 11) Before and Immediately After IV Injection of Contrast Agent

Location	Without Contrast	With Contrast	Enhancement
Aorta	37 ± 4	210 ± 7	173
Spleen	39 ± 5	73 ± 6	34
Liver	61 ± 5	137 ± 12	76

CHALLENGES FOR CT-BASED ATTENUATION CORRECTION

For normal biological materials the bilinear scaling method[31] of x-ray-based attenuation correction for PET/CT scanners performs satisfactorily for clinical procedures. However, there is no unique transformation from CT energies to 511 keV when the object contains a complex mixture of material components, such as CT contrast agents or metallic objects. Errors can also arise from respiratory motion, truncation of the CT field of view, and beam-hardening or scattered radiation if the patient's arms are in the field of view of the CT scan. When the PET emission sinograms are normalized by the attenuation correction factors $\alpha(x',\phi)$ in Eq. 9, it is assumed that the reciprocal of the attenuation correction factors are accurate measurements of the attenuation effects. A mismatch between the measured and true attenuation values can introduce biases and artifacts into the reconstructed PET image.

Spatial Mismatches

Spatial mismatches can arise from respiratory or other forms of patient motion between the CT and PET scans, which can also happen with positron or γ-ray based transmission scanning. CT transmission scans, however, typically are acquired with the patient holding his or her breath at peak inspiration to prevent the appearance of respiratory-induced artifacts in the CT image. Unfortunately, the anatomical features in a CT scan acquired at end-inspiration will not spatially match the respiratory-averaged PET scan, which has a typical duration of 30 to 45 minutes. Subsequent use of end-inspiration CT scans

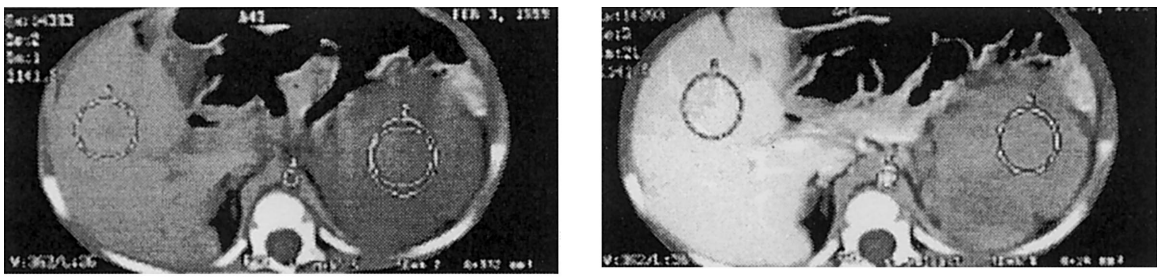

Fig 11. Transaxial CT images at the level of the liver (a) before and (b) immediately after IV injection of contrast agent. Circular ROI were defined as indicated to estimate tissue attenuation coefficients. Data courtesy of Martin Charon, MD.

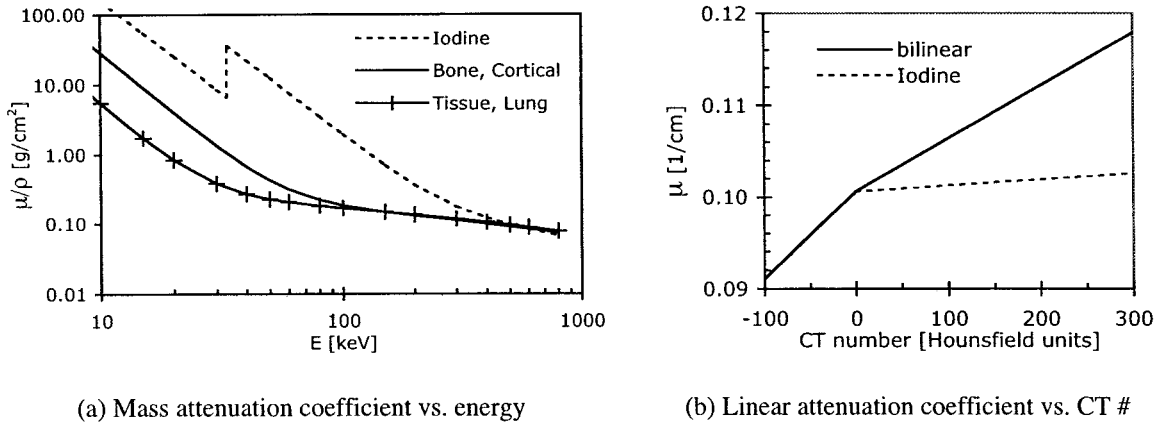

Fig 12. Comparison of scaling of attenuation coefficients for iodine for other materials. (a) The mass attenuation coefficient is significantly enhanced at CT photon energies for iodine, while at 511 keV it is similar to other materials.[11] (b) Comparison of the linear attenuation coefficient (at 511 keV) versus. CT number predicted by the bilinear method compared with the true value for iodine.[1]

to correct respiratory-averaged PET scans for attenuation will introduce misregistration artifacts into the reconstructed PET emission image.[39,40] This effect is illustrated in Fig 10.

One compromise that can be made is to acquire the CT scan during partial or full expiration to match the average PET position. This may degrade the diagnostic quality of the CT image, but provides a better spatial match with the PET emission image. Other techniques have been proposed, including respiratory gating emission scan or respiratory motion tracking coupled with list-mode acquisition of the emission data. These approaches, however, will involve more complex hardware and/or data processing algorithms.

Contrast Agents

Quantitative mismatches arise from the incorrect conversion of CT numbers to linear attenuation coefficients at 511 keV.[24] The presence of contrast agents or metal objects in the patient during the CT scan can cause significant errors in the 511 keV attenuation map when using the bilinear or hybrid conversion methods.[41,42] In cancer imaging, iodinated intravenous contrast agents are necessary for detection of lesions in solid organs and to better identify lymph nodes. Oral contrast is administered to differentiate normal from abnormal bowel and to differentiate bowel from mesenteric masses. Concurrent intravenous and oral contrast enhancement is therefore critical for cancer staging with CT and often necessary for correlation with FDG PET staging studies.

Intravenous contrast agents have iodine concentrations of 300 to 380 mg/mL. Depending on the phase of vascular enhancement desired, CT imaging protocols will call for 100 to 200 mL of contrast agent to be injected intravenously as a bolus at a rate of 1.5 to 5 mL/s. Clearance from the vascular space and tissues

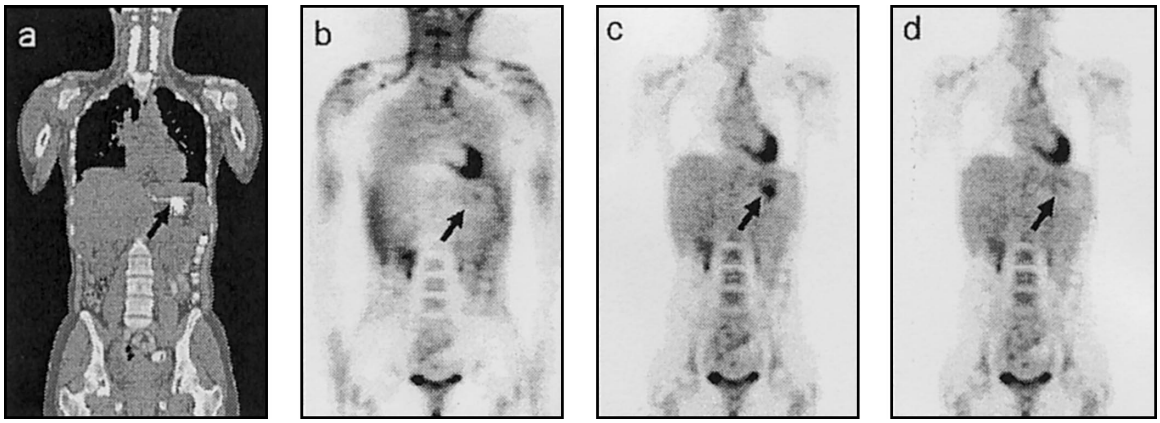

Fig 13. Effect of contrast agent accumulation. (a) CT image showing regions of highly enhanced CT values due to a focal accumulation oral contrast in stomach (arrow). (b) PET image without attenuation correction. (c) PET image with CT-based attenuation correction using the hybrid method. (d) PET image using CT-based attenuation correction with contrast-agent enhanced CT values set to 0 HU by using an automated region-growing segmentation algorithm.[43] Courtesy of Jonathan Carney, PhD.

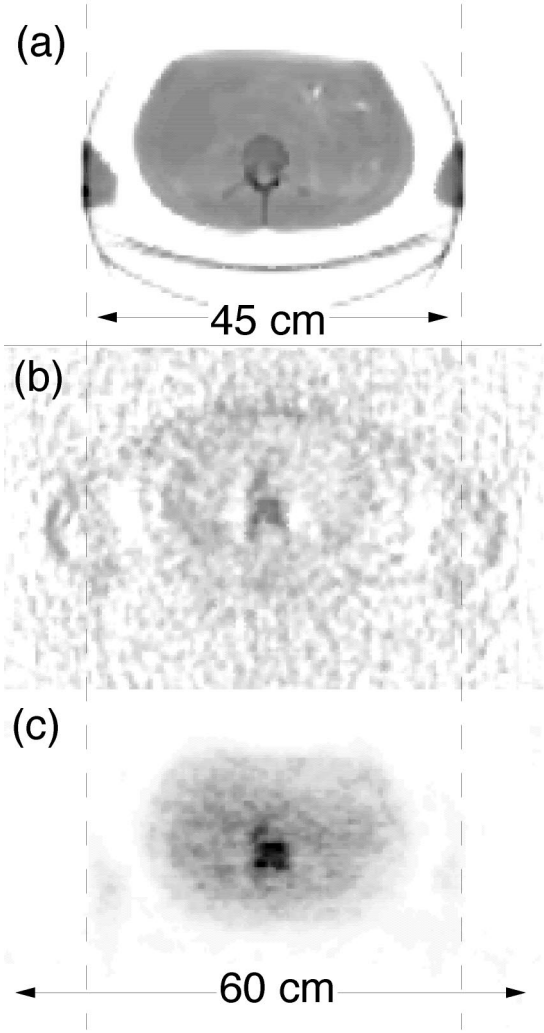

Fig 14. The problem of truncated CT attenuation information for clinical PET/CT studies. The field of view for the CT and PET scanners are 45 and 60 cm, respectively. (a) Transaxial sections through CT whole-body image volume at the level of the lower liver. Transaxial sections through PET image before (b) and after (c) CT-based attenuation correction. Dashed vertical lines indicate the CT field of view.

occurs in minutes, so the injection is performed while the patient is in the CT scanner. As they are excreted, intravenous contrast agents accumulate in the collecting system of the kidneys, ureters, and bladder. Oral contrast agents are usually based on barium. They persist for a day or two and can accumulate focally in different regions of the gastrointestinal tract. To opacify the entire gastrointestinal tract, up to three doses may need to be administered, starting the night before the CT scan.

Contrast agents have a high atomic number ($Z = 53$ for iodine and 56 for barium), which results in a high mass attenuation coefficient at x-ray photon energies because of photoelectric absorption as described by Eq. 2. The photoelectric effect is so pronounced for these materials that the use of 10 g of iodine can produce easily visible differences on a CT image as illustrated in Fig 11.

In the absence of intravenous contrast, vascularized tissues have CT numbers in the range of 30 to 60 HU. Immediately after a bolus injection of iodinated contrast media, the CT numbers can reach up to 200 to 300 HU for the aorta or the renal cortex (Table 2).

At 511 keV the mass attenuation coefficient of iodine and barium is essentially the same as water or tissue (Fig 12a). The values of contrast-enhanced CT values range from 0 to 300 HU, although the true linear attenuation coefficient at 511keV for iodine varies little, as shown by Fig 12b. Thus any scale factor that correctly predicts the attenuation coefficient at 511 keV for bone or soft tissue will overestimate the attenuation at 511 keV for contrast agents.

Focal accumulation of contrast agent, for example in an artery during a bolus injection, can result in artifactual hot spots in the PET emission image in the same location. An example of this effect is given in Fig 13. for oral contrast accumulation in the stomach. An accumulation of contrast agent, however, does not affect PET emission images that are not attenuation corrected (Fig 13b). For contrast agents these effects are only visible in the emission image in very high concentrations.[1] Even at lower concentrations, however, with the overlap in CT values for contrast-enhanced and non-enhanced tissues it is difficult to decide on the true attenuation coefficient based solely on the CT number. PET and CT image fusion, or reconstructing the emission data without attenuation correction, can be used to guide the physician as to whether the hot spot in the attenuation corrected PET image is real or is an artifact caused by quantitative errors in the attenuation image.

Segmentation methods of converting CT numbers to attenuation coefficients that correctly scale contrast-enhanced CT images have been proposed for intravenous[43] and oral[44] agents (Fig 13d). With these methods, however, proper segmentation of the contrast-enhanced regions is critical, just as it is for the segmentation-based conversion method described above.

Truncation Artifacts

Typical PET scans require imaging times of 30 to 45 minute, or longer, and are acquired with patients placing their arms down beside their torso for comfort. However, clinical CT scans are acquired over much shorter procedure times and can be acquired with the patient's arm lifted overhead and out of the field of view to improve image quality. As a result, a PET scanner has a field of view diameter of approximately 55 to 60 cm to accommodate most patient sizes in comparison with a 45 to 50 cm diameter field of view for CT. For procedures with PET/CT scanners, the same patient orientation must be used for both the PET and CT scans, which usually means that the arms are in the field of view for both. This often leads to

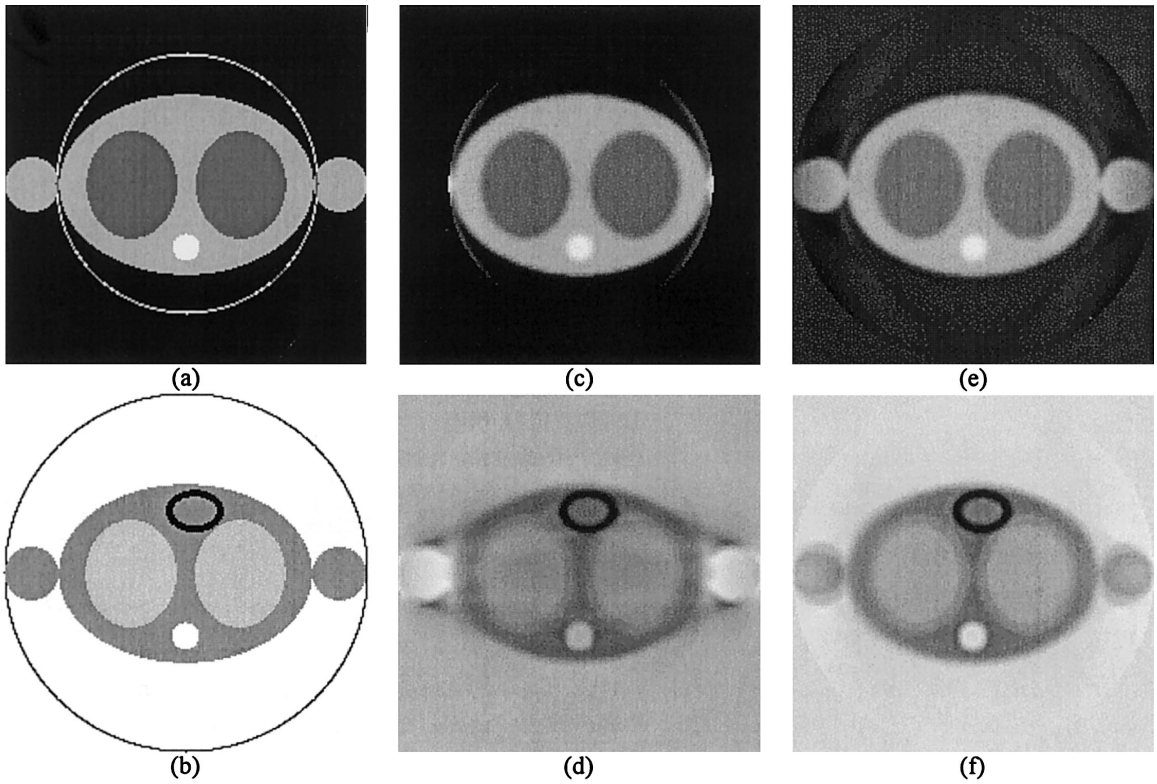

Fig 15. Simulation of the effect of CT truncation artifacts on CT-based attenuation correction of PET emission data. Top row: attenuation (CT) images displayed with a grey scale (denser objects are brighter). Bottom row: corresponding emission (PET) images displayed with an inverse grey scale (darker regions correspond to increased tracer uptake). (a) True attenuation image, showing simulated torso cross-section with arms, lungs, and spine. A typical 50 cm CT field-of-view is indicated by the circle. (b) True emission image, with simulated uptake by torso, arms, lungs, and heart (no uptake by spine). A typical 70 cm PET field-of-view is indicated by the circle. (c) Transmission image reconstructed from truncated CT sinogram. (d) Emission image reconstructed with atenuation correction based on forward-projected attenuation correction factors from (c). (e) Transmission image reconstructed from simple extrapolation of truncated CT sinogram. (f) Emission image reconstructed with attenuation correction based on forward-projected attenuation correction factors calculated from figure (e).

truncation of the smaller diameter CT image, which introduces truncation artifacts peaked at the edge of the CT image. The effects of these edge artifacts on the PET emission image, however, generally are smaller than expected, particularly if an iterative transmission reconstruction algorithm is used to reconstruct the incomplete CT data. These effects are illustrated in Fig 14.

An ameliorating factor is that although the attenuation map calculated from a truncated CT image may have errors, the degree of truncation is relatively small and

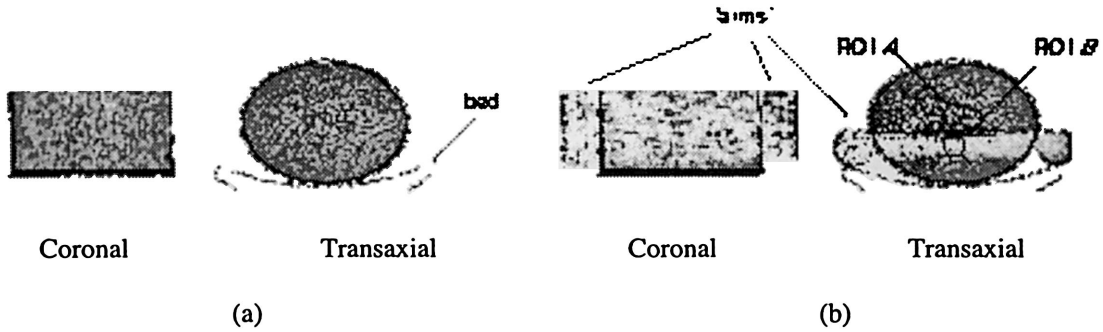

Fig 16. Artifacts arising from a combination of beam hardening and scater build-up in a CT study of a phantom simulating the abdomen with (a) and without (b) arms (5 cm diameter water bottles) in the field of view.

most of the attenuation correction factors, $\alpha(x',\phi)$, can be correctly calculated from the truncated projection data $p(x',\phi)$ (Eq. 5) data by simply using Eq. 8, where the attenuation image $\mu(x,y)$ is estimated as "best as possible." In other words the attenuation image $\mu(x,y)$ can be estimated by first extrapolating the truncated transmission sinograms $p(x',\phi)$, followed by filtered backprojection, or by more simply using iterative reconstruction of the truncated transmission sinograms as proposed by Carney et al.[45] This is illustrated in Fig 15 with simulated noiseless CT and PET data, where the effects of truncating the transmission images (top row) are shown on the corresponding emission images (bottom row) for typical CT and PET fields of view (50 and 70 cm, indicated by circles). The truncated CT transmission image (Fig 15c) introduces striking artefacts in the corresponding emission image (Fig 15d). A simple extrapolation of the truncated sinograms leads to a more accurate reconstruction of the transmission image (Fig 15e), which leads to a more accurate attenuation corrected emission image (fig 15f). The use of iterative image reconstruct methods, such as OSEM, to reconstruct attenuation images from truncated transmission sinograms leads to images similar to figure 15e.[46]

Beam-Hardening Artifacts

A second effect introduced by keeping the patient arms in the field of view is an increase in beam-hardening and scatter-induced artifacts in the CT image. These distortions, which can have a similar appearance, will propagate into the PET emission image. These effects are illustrated with an abdominal test phantom containing aqueous ^{18}F with a concentration of 4 kBq/mL, typical of a whole body FDG PET scan. Post-injection CT scans are shown in Fig 16, where uncorrected beam hardening and scatter build-up reduces measured attenuation along lines of high attenuation between the arms (Fig 16b). The CT values for the phantom without arms was -1.5 ± 0.6 HU for regions of interest (ROI) A and B. When the arms were placed in the field of view, measured attenuation for ROI B dropped to -13 ± 3 HU while ROI A remained unaffected (-1.0 ± 0.8 HU). The effect on reconstructed PET emission data were assessed for the same ROIs. The presence of arms decreased the average value for ROI B from 4.8 ± 0.4 (arbitrary units) to 4.0 ± 0.6 (a.u.), while the average value for ROI A decreased from 4.7 ± 0.3 (a.u.) to 4.2 ± 0.3 (a.u.).

With the decreased whole body scan time afforded by the x-ray transmission source, and the improved sensitivity of modern PET scanners, it may be possible in many cases to perform the PET scan with the patient's arms overhead and out of the field of view. This has two potential advantages: the beam-hardening (or x-ray scatter) and truncation artifacts are reduced, and the attenuation for the PET emission scans is reduced, thus also reducing the necessary emission scan time.

SUMMARY

In this article we have reviewed the physics of x-ray-based attenuation correction for PET/CT scanners. All manufacturers of PET/CT scanners incorporate x-ray CT-based attenuation correction algorithms in their systems, and for some PET/CT scanners it is the only option offered. The bilinear and hybrid scaling methods work well for clinical procedures where only biological materials are being imaged. There are remaining challenges, however, that can cause errors in the converted attenuation correction factors caused by contrast agents and respiratory motion as well as truncation and beam hardening from the patient's arms remaining in the field of view. Errors that are present in the CT-based attenuation image have the potential of introducing bias or artifacts in the attenuation-corrected PET emission image. Proper interpretation of PET emission images corrected for attenuation by using the CT image relies on an understanding of the potential artifacts. In cases where an artifact or bias is suspected, careful inspection of all three available images (CT and PET emission with and without attenuation correction) using image fusion where appropriate is recommended.

ACKNOWLEDGMENTS

We would like to acknowledge the contributions of David Townsend, Jonathan Carney, Michel Defrise, Christian Michel, Claude Comtat, Charles Watson, Charles Stearns, Chuanyong Bai, Hubert Vesselle, and Jeffery Fessler in helpful discussions.

REFERENCES

1. Beyer T: Design, construction and validation of a combined PET/CT tomograph for clinical oncology. Doctoral thesis, University of Surrey, Surrey, UK, 1999

2. Beyer T, Townsend DW, Brun T, et al: A combined PET/CT scanner for clinical oncology. J Nucl Med 41:1369-1379, 2000

3. Kinahan PE, Townsend DW, Beyer T, et al: Attenuation correction for a combined 3D PET/CT scanner. Med Phys 25:2046-2053, 1998

4. Sorenson JA, Phelps ME: Physics in Nuclear Medicine (ed 2). Orlando, Grune & Stratton, 1987

5. Bai C, Kinahan PE, Brasse D, et al: Effects of attenuation on tumor detection in wholebody PET oncology imaging. J Nucl Med (in press), 2003

6. Bai C, Kinahan PE, Brasse D, et al: Predicting the appearance of whole-body PET oncology images that are not corrected for attenuation. J Nucl Med 42:140P, 2001 (abstract)

7. Wahl RL: To AC or not AC: That is the question. J Nucl Med 40:2025-2028, 1999

8. Hubbell JH: Review of photon interaction cross section data in the medical and biological context. Phys Med Biol 44:R1-R22, 1999

9. Hubbell JH: Photon Cross Sections, Attenuation Coefficients, and Energy Absorption Coefficients From 10 keV to 100 GeV. Washington D.C.: National Bureau of Standards, NSRDS-NBS 29, 1969

10. Evans RD: The Atomic Nucleus. New York: McGraw-Hill, 1955

11. Hubbell JH, Seltzer SM: Tables of X-Ray Mass Attenuation Coefficients and Mass Energy-Absorption Coefficients. National Institute of Standards and Technology, Gaithersburg, MD, July 5, 2001, 1997), available at: http://physics.nist.gov/xaamdi, Accessed January 2003

12. ICRU: Tissue Substitutes in Radiation Dosimetry and Measurement. Bethesda, MD: International Commission on Radiation Units and Measurements 44, 1989

13. Kak AC, Slaney M: Principles of Computerized Tomographic Imaging. New York, IEEE Press, 1988

14. Ollinger JM, Fessler JA: Positron emission tomography. IEEE Signal Processing Magazine 14:43-55, 1997

15. Leahy R, Qi J: Statistical approaches in quantitative positron emission tomography. Stat Comput 10:147-165, 2000

16. Joseph PM, Spital RD: A method for correcting bone induced artifacts in computed tomography scanners. J Comput Assist Tomogr 2:100-108, 1978

17. Comtat C, Kinahan PE, Defrise M, et al: Fast reconstruction of 3D PET data with accurate statistical modeling. Proceedings of the 1998 IEEE Nuclear Science Symposium and Medical Imaging Conference, 1997, pp CDROM

18. Bailey DL: Transmission scanning in emission tomography. Eur J Nucl Med 25:774-787, 1998

19. Bendriem B, Townsend DW: The Theory and Practice of 3D PET. Dordrecht, Kluwer Academic Publishers, 1998

20. Xu M, Cutler PD, Luk WK: Adaptive segmented attenuation correction for whole-body PET imaging. IEEE Trans Nucl Sci NS 43:331-336, 1996

21. Erdogan H, Fessler JA: Ordered subsets algorithms for transmission tomography. Phys Med Biol 44:2835-2851, 1999

22. de Kemp RA, Nahmias C: Attenuation correction in PET using single photon transmission measurement. Med Phys 21:771-778, 1994

23. Karp JS, Muehllehner G, Qu H, et al: Singles transmission in volume-imaging PET with a 137Cs source. Phys Med Biol 40:929-944, 1995

24. Bai C, Kinahan PE, Brasse D, et al: Post-injection single photon transmission tomography with ordered-subset algorithms for wholebody PET imaging. IEEE Trans Nucl Sci 49:74-81, 2002

25. Smith RJ, Karp JS, Muehllehner G, et al: Singles transmission scans performed post-injection for quantitative whole body PET imaging. IEEE Trans Nucl Sci 44:1329-1335, 1997

26. Watson CC, Schaefer A, Luk WK, et al: Clinical evaluation of single-photon attenuation correction for 3D whole-body PET. IEEE Trans Nucl Sci 46:1024-1031, 1999

27. Comtat C, Kinahan PE, Fessler JA, et al: Clinically feasible reconstruction of 3D whole-body PET/CT data using blurred anatomical labels. Phys Med Biol 47:1-20, 2002

28. Fleming JS: A technique for using CT images in attenuation correction and quantification in SPECT. Nucl Med Commun 10:83-97, 1989

29. Hasegawa BH, Lang TF, Brown EL, et al: Object specific attenuation correction of SPECT with correlated dual-energy X-ray CT. IEEE Trans Nucl Sci NS-40:1242-1252, 1993

30. LaCroix KJ, Tsui BMW, Hasegawa BH, et al: Investigation of the use of X-ray CT images for attenuation compensation in SPECT. IEEE Trans Nucl Sci NS-41:2793-2799, 1994

31. Blankespoor SC, Wu X, Kalki JK, et al: Attenuation correction of SPECT using X-ray CT on an emission-transmission CT system: Myocardial perfusion assessment. IEEE Trans Nucl Sci 43:2263-2274, 1996

32. Robinson PJ, Kreel L: Pulmonary tissue attenuation with computed tomography: Comparison of inspiration and expiration scans. J Comput Assist Tomogr 3:740-748, 1979

33. Burger C, Goerres G, Schoenes S, et al: PET attenuation coefficients from CT images: Experimental evaluation of the transformation of CT into PET 511-keV attenuation coefficients. Eur J Nucl Med Mol Imag 29:922-927, 2002

34. Bai C, Shao L, Da Silva AJ: CT-based attenuation correction for PET/CT scanners. Proceedings of the IEEE Nuclear Science Symposium and Medical Imaging Conference. Norfolk, VA, November 11-16, 2002

35. Charron M, Beyer T, Bohnen NN, et al: Image analysis in oncology patients studied with a combined PET/CT scanner. Clin Nucl Med 25:905-910, 2000

36. Kamel E, Hany TF, Burger C, et al: CT vs 68Ge attenuation correction in a combined PET/CT system: Evaluation of the effect of lowering the CT tube current. Eur J Nucl Med 29:346-350, 2002

37. Nakamoto Y, Osman M, Cohade C, et al: PET/CT: comparison of quantitative tracer uptake between germanium and CT transmission attenuation-corrected images. J Nucl Med 43:1137-1143, 2002

38. Alvarez RE, Macovski A: Energy-selective reconstructions in X-ray computerized tomography. Phys Med Biol 21:733-744, 1976

39. Isoardi RA, Comtat C, Frouin V, et al: Simulating respiratory motion in whole-body PET imaging with the MCAT phantom. Proceedings of the IEEE Nuclear Science Symposium and Medical Imaging Conference. Norfolk, VA, November 11-16, 2002

40. Goerres GW, Kamel E, Heidelberg TN, et al: PET-CT image co-registration in the thorax: Influence of respiration. Eur J Nucl Med Mol Imaging 29:351-360, 2002

41. Antoch G, Freudenberg LS, Egelhof T, et al: Focal tracer uptake: A potential artifact in contrast-enhanced dual-modality PET/CT scans. J Nucl Med 43:1339-1342, 2002

42. Goerres GW, Hany TF, Kamel E, et al: Head and neck imaging with PET and PET/CT: Artefacts from dental metallic implants. Eur J Nucl Med Mol Imag 29:367-370, 2002

43. Tang HR, Brown JK, Da SAJ, et al: Implementation of a combined X-ray CT-scintillation camera imaging system for localizing and measuring radionuclide uptake: Experiments in phantoms and patients. Proceedings of the IEEE Trans Nucl Sci, 1999, pp 551-557

44. Carney J, Beyer T, Brasse D, et al: CT-based attenuation correction for PET/CT scanners in the presence of contrast agent. Proceedings of the IEEE Nuclear Science Symposium and Medical Imaging Conference, Norfolk, VA, November 11-16, 2002

45. Carney J, Townsend D, Kinahan PE, et al: CT-based attenuation correction: The effects of imaging with the arms in the field of view. J Nucl Med 42:56P, 2001(abstr)

46. Nuyts J, Michel C, Bai C: Personal communications, 2001